

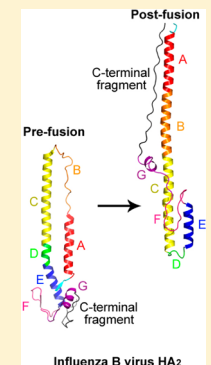
## Structural Insights into the Membrane Fusion Mechanism Mediated by Influenza Virus Hemagglutinin

Fengyun Ni,<sup>†,‡</sup> Xiaorui Chen,<sup>†</sup> Jun Shen,<sup>‡</sup> and Qinghua Wang<sup>\*,†</sup>

<sup>†</sup>Verna and Marrs McLean Department of Biochemistry and Molecular Biology, Baylor College of Medicine, One Baylor Plaza, Houston, Texas 77030, United States

<sup>‡</sup>Department of Bioengineering, Rice University, Houston, Texas 77005, United States

**ABSTRACT:** Membrane fusion is involved in many fundamental cellular processes and entry of enveloped viruses into host cells. Influenza type A virus HA has long served as a paradigm for mechanistic studies of protein-mediated membrane fusion via large-scale structural rearrangements induced by acidic pH. Here we report the newly determined crystal structure of influenza B virus HA<sub>2</sub> in the postfusion state. Together with a large number of previously determined prefusion structures of influenza A and B virus HA and a postfusion structure of influenza A/H3N2 HA<sub>2</sub>, we identified conserved features that are shared between influenza A and B virus HA in the conformational transition and documented substantial differences that likely influence the detailed mechanisms of this process. Further studies are needed to dissect the effects of these and other structural differences in HA conformational changes and influenza pathogenicity and transmission, which may ultimately expedite the discovery of novel anti-influenza fusion inhibitors.



Membrane fusion, the merger of two separate lipid bilayers, is involved in many fundamental cellular processes and entry of enveloped viruses into host cells. Cellular membrane fusion is mediated by the SNARE family members, while viral membrane fusion is accomplished by three classes of viral fusion proteins. Class I is represented by influenza virus hemagglutinin (HA), Ebola virus GP1/GP2, and human immunodeficiency virus-1 gp120/gp41. Class II is exemplified by dengue and yellow fever virus glycoprotein E and vesicular stomatitis virus glycoprotein G. Class III includes herpes simplex virus-1 gB protein.<sup>1–4</sup> Recent studies have revealed a common mechanism by which cellular and viral fusion proteins catalyze membrane fusion through the formation of hairpin structures at the postfusion state.<sup>1–5</sup> This is achieved via the zipping together of t-SNARE and v-SNARE molecules or large-scale conformational changes of viral fusion proteins. The conformational changes of viral fusion proteins are triggered by either low pH or receptor binding.<sup>1–6</sup>

Influenza type A virus HA has long served as a paradigm for mechanistic studies of protein-mediated membrane fusion.<sup>6–8</sup> HA is initially synthesized as a single polypeptide chain (HA<sub>0</sub>) and forms a stable homotrimer that is anchored on the envelope of the virus by a type I transmembrane domain located at the extreme C-terminus. Its cleavage by intracellular proteases gives rise to a prefusion state HA containing disulfide-bonded HA<sub>1</sub> and HA<sub>2</sub>. This cleavage of HA<sub>0</sub> is essential for viral infectivity and pathogenicity.<sup>6,7,9–12</sup> HA mutants with elevated pH values for membrane fusion have been mapped exclusively to (a) HA<sub>1</sub>–HA<sub>1</sub> interfaces, (b) HA<sub>1</sub>–HA<sub>2</sub> interfaces, (c) the fusion peptide and its surrounding region, and (d) the region around the B-loop, suggesting that these regions are involved in

structural rearrangements of HA in the transition from the prefusion state to the postfusion state.<sup>13–15</sup>

The crystal structures of influenza A/H3N2 virus HA in uncleaved precursor (HA<sub>0</sub>),<sup>16</sup> cleaved prefusion (HA),<sup>17</sup> and postfusion (HA<sub>2</sub>)<sup>15,18</sup> states have shed a great deal of light on the molecular mechanism of HA-mediated membrane fusion. Comparison of the structures of precursor HA<sub>0</sub> and cleaved prefusion HA has revealed how the burial of the fusion peptide at the extreme N-terminus of HA<sub>2</sub> in a negatively charged cavity formed by His-17 of HA<sub>1</sub> and Asp-109 and Asp-112 of HA<sub>2</sub> primes the molecule for low-pH-induced conformational changes.<sup>16</sup> Indeed, a recent study using single influenza virions has revealed that the exposure of the buried fusion peptide is a rate-limiting step toward hemifusion.<sup>19</sup> In addition, structural comparison of prefusion HA and postfusion HA<sub>2</sub> has uncovered the extent of the conformational changes between these two different states. However, the molecular forces that underlie such large-scale conformational changes remain poorly understood.

The success of the clinical drug T-20 in treating HIV-1 patients<sup>20</sup> clearly demonstrated that inhibitors of fusion can be an effective antiviral strategy. This strategy is especially valid given the highly conserved nature of the membrane fusion mechanism across different viruses. Indeed, the stem region of influenza virus HA, which contains the N- and C-terminal fragments of HA<sub>1</sub> and the full-length HA<sub>2</sub> and is the actual membrane fusion agent, is the most conserved region in terms of structures and functions.<sup>21</sup> Antibodies that recognize this

Received: November 12, 2013

Revised: January 16, 2014

Published: January 16, 2014

stem region were found to have broad neutralization activities across different types and subtypes of influenza virus.<sup>22–24</sup> An in-depth understanding of the structural basis of the HA-mediated membrane fusion mechanism, in particular the initiation, sequential events, and intermediates of the structural rearrangements, will undoubtedly expedite the discovery and development of novel anti-influenza fusion inhibitors.<sup>8</sup>

Influenza B virus is another major member of the Orthomyxoviridae family and, together with influenza A virus subtypes H1N1, H2N2, and H3N2, is responsible for seasonal influenza epidemics. Influenza B virus HA shares very low levels of protein sequence identity with influenza A virus HA, at only ~20% for HA<sub>1</sub> and ~29% for HA<sub>2</sub> residues 31–181. We have determined a number of crystal structures of influenza B virus HA that provide significant insights into the evolution, receptor binding, and antigenicity of this protein.<sup>25–27</sup> Here, we report the determination of the crystal structure of influenza B virus HA<sub>2</sub> in the postfusion state (Table 1). Systematic structural

**Table 1. Data Collection and Refinement Statistics of Influenza B Virus HA<sub>2</sub><sup>a</sup>**

Data Collection	
wavelength (Å)	1.127
resolution range (Å)	37.76–2.45 (2.54–2.45)
space group	R32
unit cell	
<i>a</i> , <i>b</i> , <i>c</i> (Å)	48.2, 48.2, 354.9
$\alpha$ , $\beta$ , $\gamma$ (deg)	90, 90, 120
total no. of reflections	25553
no. of unique reflections	5617 (584)
multiplicity	4.5 (4.4)
completeness (%)	89.43 (94.96)
mean $I/\sigma(I)$	15.8 (5.2)
Wilson $B$ factor (Å <sup>2</sup> )	40.4
$R_{\text{sym}}$ (%)	0.053 (0.210)
Refinement	
$R_{\text{crystal}}$ (%)	0.255 (0.273)
$R_{\text{free}}$ (%)	0.268 (0.333)
no. of atoms	1111
macromolecules	1084
waters	27
no. of protein residues	142
root-mean-square deviation	
bond lengths (Å)	0.005
bond angles (deg)	0.81
Ramachandran favored (%)	91.0
Ramachandran outliers (%)	2.9
Clashscore	34.1
average $B$ factor (Å <sup>2</sup> )	53.2
macromolecules	53.4
solvent	44.4

<sup>a</sup>Statistics for the highest-resolution shell are given in parentheses.

comparison of known influenza A and B virus HA in prefusion and postfusion states has revealed critical new insights into the molecular basis for the conformational changes upon exposure to low pH.

## MATERIALS AND METHODS

**Expression, Purification, Crystallization, and Structural Determination.** HA<sub>2</sub> residues 31–181 of influenza B/Yamagata/73 were cloned into vector pET-45b with an

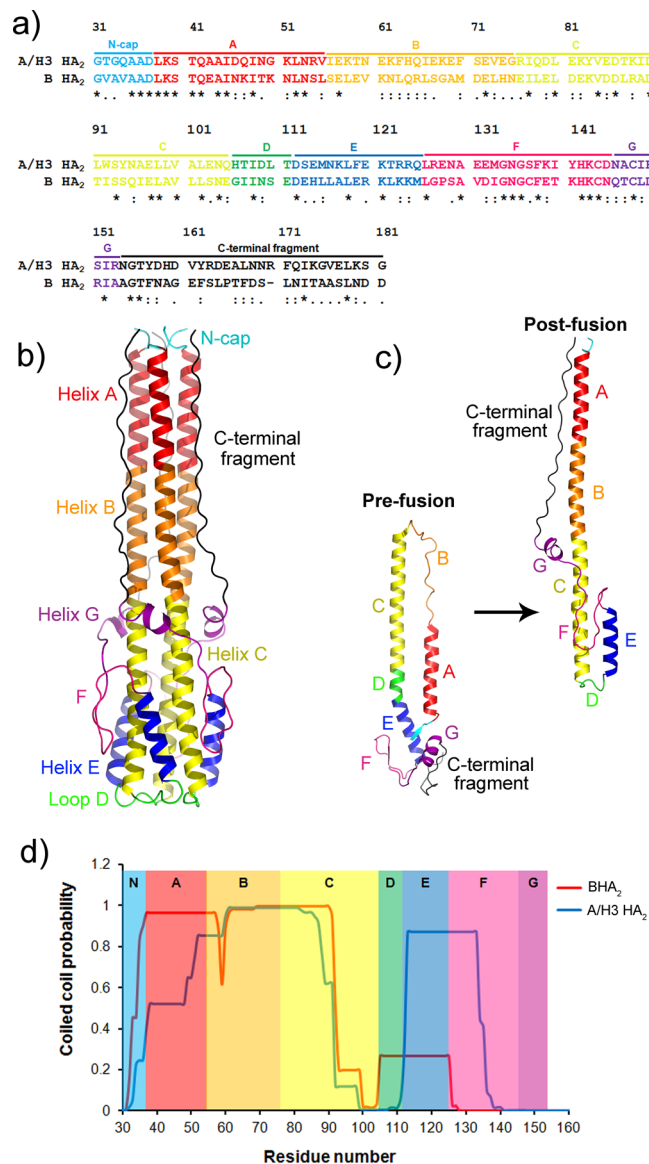


**Figure 1.** Overall structure of influenza B virus HA<sub>2</sub>. (a) Sequence alignment of influenza A/H3N2 and B virus HA<sub>2</sub> in the region of residues 31–181. The sequence similarity is indicated by the following codes: asterisks for identity, colons for a high degree of similarity, periods for similarity, and spaces for no similarity. (b) HA<sub>2</sub> trimer structure of influenza B virus HA<sub>2</sub>. (c) Illustration of the conformational changes of influenza B virus HA<sub>2</sub> from the prefusion state (PDB entry 3BT6) to the postfusion state. The structures are aligned at helix C, the only region that is not rearranged during the transition. The HA<sub>1</sub> subunit of the prefusion structure has been omitted for the sake of clarity. (d) Comparison of the helical propensity of influenza A/H3N2 and B virus HA<sub>2</sub> in the region of residues 31–160. Panels a–c use the same coloring scheme.

N-terminal six-histidine tag and expressed in *Escherichia coli* Rosetta 2(DE3)pLysS (Novagen). Expressed HA<sub>2</sub> was purified using cobalt resin (Thermo Scientific) and size-exclusion chromatography (Superdex 200 10/300 GL, GE Healthcare). Purified HA<sub>2</sub> was concentrated to 10 mg/mL in 10 mM Hepes (pH 7.6), and crystals were grown at 290 K by the hanging drop method in a reservoir solution of 0.1 M ammonium citrate and 13.5% PEG 3350 (pH 7.0). The diffraction data were collected using the 14-BMC beamline (BioCARs) at the Advanced Photon Source (Chicago, IL), indexed and

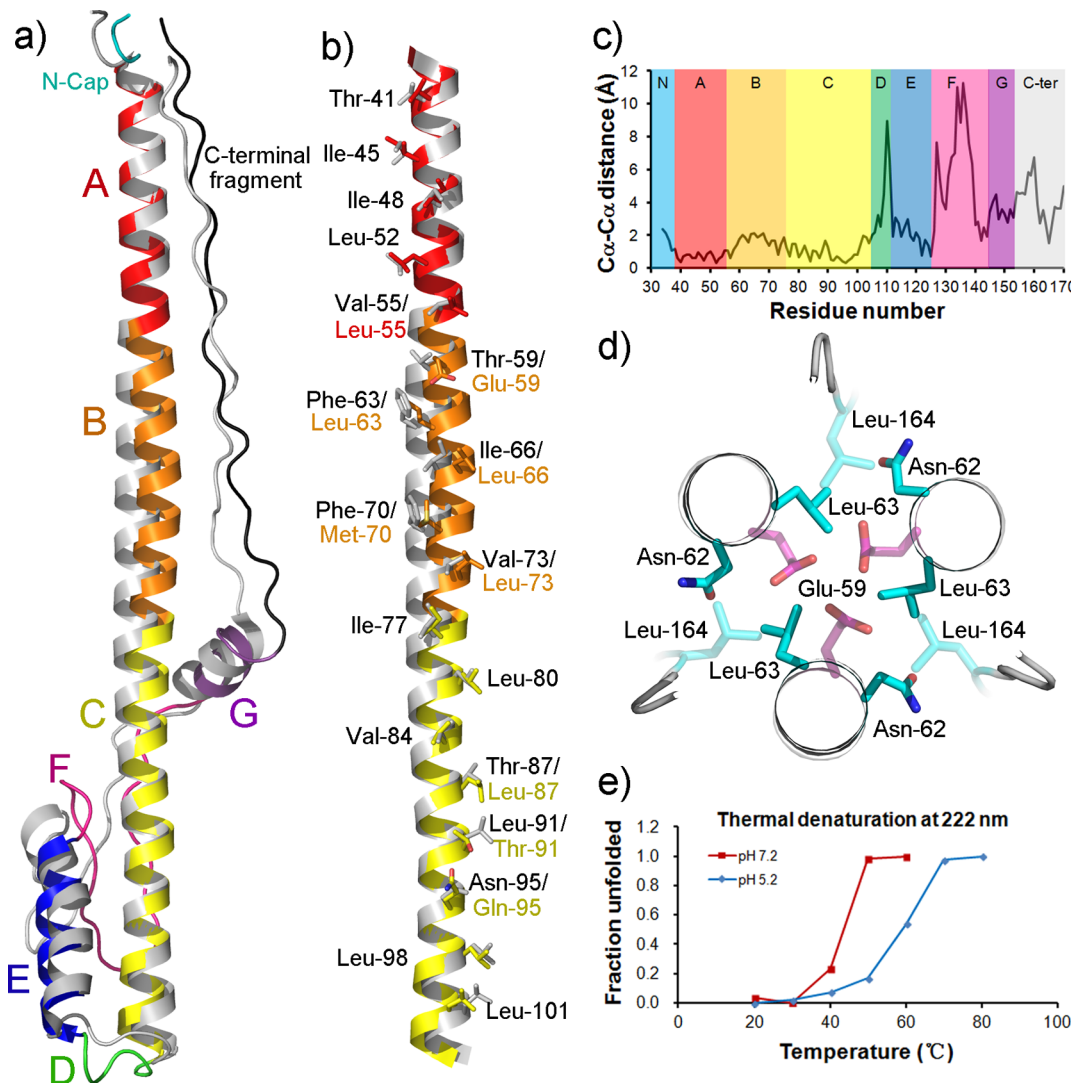


**Figure 2.** Protein core of HA<sub>2</sub>. (a) Alignment of influenza A/H3N2 and B virus HA<sub>2</sub> structures. The loop regions have the largest structural differences, while region B has larger structural deviations in the central three-helix coiled coil. (b) Comparison of the residues that constitute the protein core of influenza A/H3N2 and B virus HA<sub>2</sub>. Because this study mostly focuses on HA<sub>2</sub>, the residues on HA<sub>2</sub> will be mentioned in the format of, for example, Thr-41, throughout the text. Residues on HA<sub>1</sub> are specifically indicated as, for instance, HA<sub>1</sub> His-17. (c) Plot of C<sub>α</sub>-C<sub>α</sub> distances between influenza A/H3N2 and B virus HA<sub>2</sub>. (d) Burial of Glu-59 in the protein core of influenza B virus HA<sub>2</sub>. (e) Thermal denaturation of influenza B virus HA<sub>2</sub> at pH 5.2 and 7.2. Panels a–c use the same coloring scheme as Figure 1a.

integrated by using MOSFLM,<sup>28,29</sup> scaled by SCALA, and truncated to structure factor amplitude by TRUNCATE in CCP4.<sup>30</sup> Five percent of unique reflections omitted from refinement were used as the test set for calculating the R<sub>free</sub> values.

The long helix from the postfusion structure of influenza A/H3N2 virus HA<sub>2</sub> [Protein Data Bank (PDB) entry 1QU1],<sup>18</sup> including residues 37–105, was pruned to C<sub>β</sub> atoms by CHAINSAW in the CCP4 suite and served as the search model for molecular replacement by the AutoMR module implemented in PHENIX.<sup>31</sup> There is one polypeptide chain of HA<sub>2</sub> in the asymmetric unit. The biological HA<sub>2</sub> trimer was generated by symmetry operation. The resulting σ-weighted 2F<sub>o</sub> – F<sub>c</sub> map showed clear densities for the rest of the protein that were built into the density by COOT.<sup>32</sup> The model was refined by REFMAC5<sup>33</sup> in CCP4 or the Refinement module in PHENIX.<sup>31</sup> Figures for structural snapshots were generated by using Pymol.

## RESULTS

**Overall Structure of Influenza B Virus HA<sub>2</sub>.** The level of sequence identity between influenza A/H3N2 and B virus HA<sub>2</sub> is only ~29% as calculated by ClustalW2 (Figure 1a). The N-terminal region containing part of the N-cap and region A is the most conserved between them, while the most variable regions are region B and the C-terminal fragment (Figure 1a). However, both types of HA<sub>2</sub> fold into the same hairpinlike structures (Figure 1b). The N-cap domain (residues 31–37) stops the extension of the central three-helix coiled coil (Figure 1b). The central three-helix coiled coil is assembled from three segments: helix A (residues 38–55) that is a short α-helix in the prefusion state, helix B (residues 56–75) that is converted from a loop in the prefusion state, and helix C (residues 76–105) that is part of the long helix in the prefusion state (Figure 1c). This long central helix is followed by loop D (residues 106–111) that is unfolded from part of the long central helix in the prefusion state (Figure 1c). Following this loop is helix E (residues

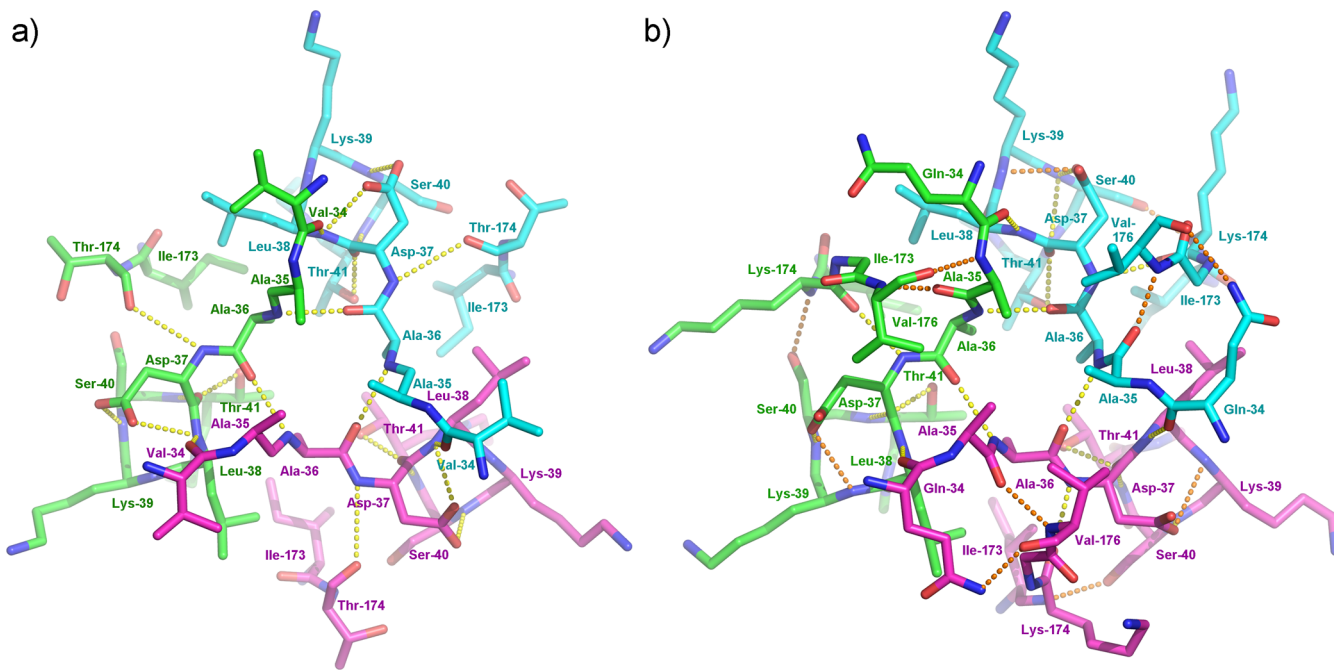


**Figure 3.** N-Cap domain. (a) Interaction network of the N-cap domain in influenza B virus HA<sub>2</sub>. Hydrogen bonds are shown as yellow dashed lines. (b) Interaction network of the N-cap domain in influenza A/H3N2 virus HA<sub>2</sub>. The hydrogen bonds that are also observed in influenza B virus HA<sub>2</sub> are shown as yellow dashed lines, while those unique to influenza A/H3N2 HA<sub>2</sub> are highlighted as orange dashed lines. The three subunits of the trimer are differently colored.

112–125) that is packed against the long central helix in an anti-parallel orientation, forming a six-helix bundle (Figure 1b,c). Loop F (residues 126–145) and helix G (residues 146–153) have relatively weaker electron densities and higher *B* factors, suggesting greater structural flexibility. Consistent with this observation, for the reported influenza A/H3N2 virus HA<sub>2</sub> structure (PDB entry 1QU1) where there are two trimers in the asymmetric unit, this region displays different conformations, including  $\alpha$ -helix,  $\beta$ -sheet, or random coil, in different chains.<sup>18</sup> The C-terminal fragment (residues 154–181) runs along the groove between the two neighboring central helices and interacts with the N-cap domain at one extreme end of the molecule (Figure 1b).

As the  $\alpha$ -helical conformation predominates the postfusion structure, we also analyzed the helical propensity of influenza A/H3N2 and B virus HA<sub>2</sub> in the region of residues 31–160 using COILS/PCOILS (<http://toolkit.tuebingen.mpg.de/pcoils>) (Figure 1d). In comparison to influenza A/H3N2 virus HA<sub>2</sub>, influenza B virus HA<sub>2</sub> clearly has a higher helical propensity in regions A and D and a lower propensity in regions E and F and exhibits a sharp dip in helical propensity in region B. This is in agreement with the observations that loop F did display a helical conformation in some of the chains in the influenza A/H3N2 virus HA<sub>2</sub> structure.<sup>18</sup>

**Protein Core.** For the central three-helix coiled coil in the postfusion structures, helices A and C can be superimposed very well between influenza A/H3N2 and B virus HA<sub>2</sub>; however, relatively larger deviations are observed in helix B (Figure 2a,c). This is consistent with the fact that region B is one of the most variable regions in sequence (Figure 1a). Among those constituting the protein core, the residues are either identical (in helix A and the N- and C-termini of helix C) or highly conserved in hydrophobicity (individually or in pairs in helix B and the middle section of helix C) (Figure 2b). The only exception is the buried Glu-59 in influenza B virus HA<sub>2</sub>,

where the corresponding residue is Thr-59 in influenza A/H3N2 virus HA<sub>2</sub>. The side chain of Glu-59 points toward the 3-fold axis and is surrounded by the hydrophilic residue Asn-62 and two large hydrophobic residues Leu-63 and Leu-164 (Figure 2d). It has been shown in Marburg virus glycoprotein GP2 that buried Glu residues result in a higher stability at low pH, leading to a hypothesis that these residues are strategically placed in sequence to favor the formation of the postfusion structure at low pH.<sup>34,35</sup> For influenza B virus HA<sub>2</sub>, we also observed a similar stabilization effect at low pH, with approximate *T<sub>m</sub>* values of 42 °C at pH 7.2 and 60 °C at pH 5.2 (Figure 2e).

**N-Cap Domain.** In influenza B virus HA<sub>2</sub>, N-terminal residues 34–37 cap the central three-helix coiled coil (Figure 3a). The side chains from the highly conserved Asp-37 form hydrogen bonds with the main chain amide groups of residues Leu-38 and Ser-40 of the same subunit (Figure 3a). In addition, the carbonyl group of Asp-37 contributes two hydrogen bonds, one with the amide group on the main chain and the other with the hydroxyl group on the side chain of Thr-41 (Figure 3a).

As the region of residues 34–37 extends toward a neighboring subunit, one hydrogen bond is observed between the carbonyl group of Val-34 and the amide group of Leu-38. In addition, the three N-caps interact with each other around the 3-fold axis of the molecule by forming two layers of hydrophobic interactions, among three Ala-36 residues and among three Ala-35 residues, and making three hydrogen bonds between the carbonyl group of Ala-36 and the amide group of the same residue on the neighboring subunit (Figure 3a). The N-cap also interacts with the C-terminal fragment by forming one hydrogen bond between the amide group of Asp-37 and the carbonyl group of Thr-174 (Figure 3a). Collectively, these interactions stabilize the N-cap domain and stop the central coiled coil structure from extending further.

In influenza A/H3N2 HA<sub>2</sub>, although most of the interactions are similarly observed, a large discrepancy is seen between the

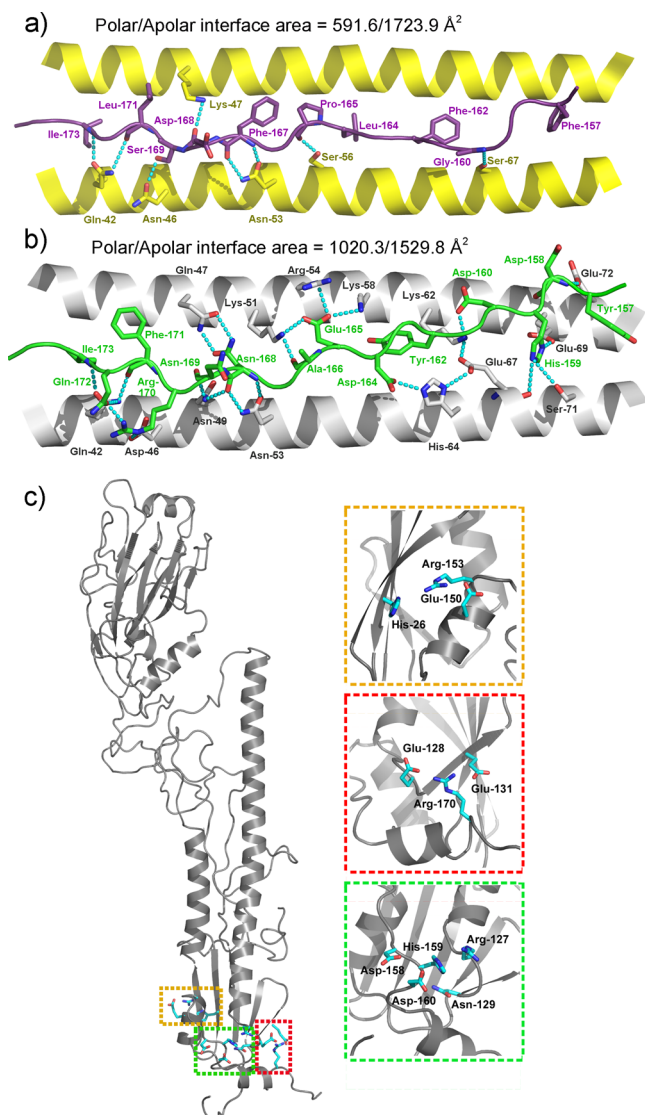


**Figure 4.** Interactions between the central helices and the C-terminal fragment. (a) Polar–apolar interface for influenza B virus HA<sub>2</sub>. (b) Polar–apolar interface for influenza A/H3N2 HA<sub>2</sub>. (c) Prefusion structure of influenza A/H3N2 HA (PDB entry 3HMG) highlighting the three ionic clusters that are absent in influenza B virus HA.

N-cap domain and the C-terminal fragment (Figure 3b). In particular, the hydrogen bonding interactions between the main chain atoms of Ala-35 and Val-176 (the carbonyl of Ala-35 and the amide of Val-176, and the amide of Ala-35 and the carbonyl of Val-176) and between the hydroxyl of Ser-40 and the amide of Lys-174 as observed in influenza A/H3N2 HA<sub>2</sub> are all absent in influenza B virus HA<sub>2</sub> (Figure 3b, highlighted as orange dashed lines).

**Interactions between the Central Helices and the C-Terminal Fragment.** The packing of the C-terminal fragment into the groove formed by neighboring central helices brings the C-terminal transmembrane domain and the N-terminal fusion peptide into the proximity of each other to promote fusion of the viral envelope and the endosomal membrane to which they each attach. We used InterProSurf (<http://curie.utmb.edu/prosurf.html>) to calculate the total surface area that is buried between the C-terminal fragment and the central helices in the postfusion structures of influenza A/H3N2 and B

virus HA<sub>2</sub>. We found that influenza B virus HA<sub>2</sub> has a total buried surface area of 2315.5 Å<sup>2</sup>, which is a bit smaller than the interface in influenza A/H3N2 virus HA<sub>2</sub> (at 2550.1 Å<sup>2</sup>). The interface in influenza B virus HA<sub>2</sub> is predominantly hydrophobic, containing a polar area of 591.6 Å<sup>2</sup> and an apolar area of 1723.9 Å<sup>2</sup> from several large hydrophobic residues such as Phe-157, Phe-162, Leu-164, Phe-167, Leu-171, and Ile-173. In contrast, influenza A/H3N2 HA<sub>2</sub> contains four hydrophobic residues, Tyr-157, Tyr-162, Phe-171, and Ile-173, and has polar and apolar interface areas of 1020.3 and 1529.8 Å<sup>2</sup>, respectively. Thus, the polar interface between the central helices and C-terminal fragment in influenza A/H3N2 HA<sub>2</sub> is almost twice as large as that of influenza B virus HA<sub>2</sub>. Via comparison to the >20 polar interactions in this region of influenza A/H3N2 virus HA<sub>2</sub>, there are only seven such interactions in influenza B virus HA<sub>2</sub> (Figure 4a,b).

The abundant polar interactions in influenza A/H3N2 virus HA<sub>2</sub> urged us to carefully inspect its prefusion structure (PDB entry 3HMG).<sup>36</sup> This revealed three clusters of ionic residues formed between the C-terminal fragment and its surrounding residues (Figure 4c). One such cluster is near the fusion peptide (in an orange box) formed by residues Glu-150 and Arg-153 with His-26. Another cluster is among Arg-170 on the C-terminal fragment and Glu-128 and Glu-131 on loop F (in the red box). The third cluster is among residues Asp-158, His-159, and Asp-160 on the C-terminal fragment and residues Arg-127 and Asn-129 on the other side of loop F (in the green box). These ionic clusters are located at regions that are to be separated during the low-pH-mediated large-scale conformational changes of HA. Similar ionic clusters are not found in the prefusion structure of influenza B virus HA.

**Six-Helix Bundle.** The six-helix bundle at the postfusion state results from a helix-to-turn transition in region D followed by the antiparallel packing of helix E against helix C. The formation of this six-helix bundle of HA is required for the formation of the hemifusion state.<sup>4,37</sup> In influenza B virus HA<sub>2</sub>, Ile-107 closely packs toward the 3-fold symmetry axis to form a tight hydrophobic core, while the next residue, Ile-108, almost sits in the middle of two adjacent helices C. The carboxyl group of Glu-105 at the C-terminus of helix C interacts with the backbone atoms of Asn-109, Ser-110, and Glu-111 in loop D from the neighboring subunit, stabilizing this arrangement by three hydrogen bonds (Figure 5a).

In influenza A/H3N2 virus HA<sub>2</sub>, Thr-107 residues form an annulus that covers the C-terminus of the coiled coil (Figure 5b). The hydroxyl groups of three Thr-107 residues form hydrogen bonds with either the carbonyl oxygen atom of Thr-107 from a neighboring subunit or the side chain of Gln-105. In comparison with that of influenza B virus HA<sub>2</sub>, the C-terminus of loop D in influenza A/H3N2 virus HA<sub>2</sub> moves farther from the central helices (Figure 5b).

The stacking orientation of helix E on the groove of two neighboring central helices C is also different in influenza A/H3N2 and B virus HA<sub>2</sub>. Helix E is straight in influenza B virus HA<sub>2</sub> but is slightly bent in influenza A/H3N2 HA<sub>2</sub> (Figure 5c,d). Structurally, this bending could be the result of the side chain packing at the interface of helix C and helix E. In influenza B virus HA<sub>2</sub>, the residues from the central helices that form the interhelical groove are smaller (Ile-92, Ser-94, and Ala-99), making a concave surface in this region. Therefore, the side chains of the hydrophobic residues (Leu-115, Leu-118, Leu-122, and Leu-126) in helix E pack snugly against this concave surface (Figure 5c). In marked contrast, the interhelical

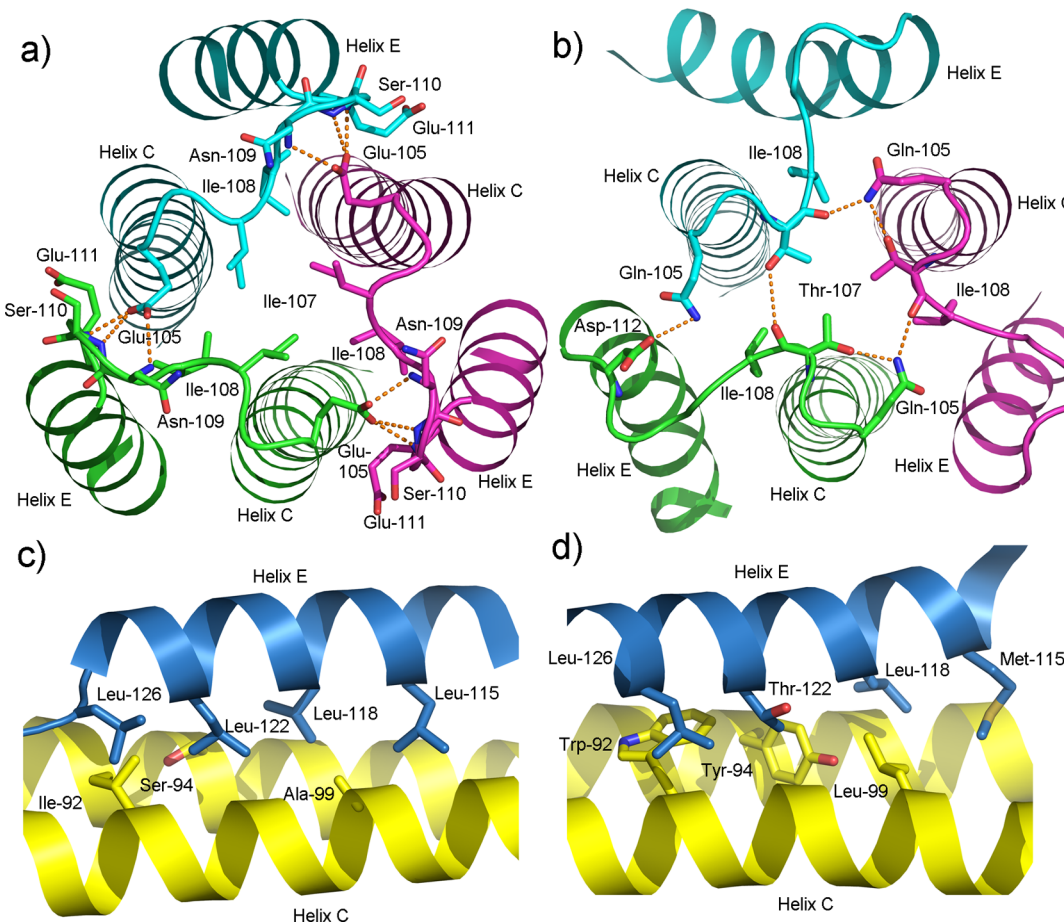


**Figure 5.** Six-helix bundle. (a) Interactions around Ile-107 in influenza B virus HA<sub>2</sub>. (b) Interactions around Thr-107 in influenza A/H3N2 virus HA<sub>2</sub>. (c) Interactions between helix C and helix E in influenza B virus HA<sub>2</sub>. (d) Interactions between helix C and helix E in influenza A/H3N2 virus HA<sub>2</sub>.

groove where helix E packs in influenza A/H3N2 virus HA<sub>2</sub> is flat because of three large residues (Trp-92, Tyr-94, and Leu-99), and the residues on helix E (Met-115, Leu-118, Thr-122, and Leu-126) have to pack slightly sideways against this groove (Figure 5d).

#### Comparisons of the Structures in the Prefusion State.

To gain more insight into the structural basis of HA-mediated membrane fusion, we further compared the prefusion structures of influenza A (H1–H3, H5, H7, H9, H13, H14, and H17) and B virus HA. When viewing from the membrane distal end of the HA molecules, we found that the HA<sub>1</sub> monomers are much closer to each other in influenza B virus HA than in influenza A virus HA (Figure 6a,b). Although group 1 and group 2 HA proteins of influenza A virus differ in the orientation of their receptor-binding (R) domains relative to those of influenza B virus HA (Table 2), their total HA<sub>1</sub>–HA<sub>1</sub> interface area is constantly smaller and the B-loop more exposed than that in influenza B virus HA (Table 2).

The large differences in the HA<sub>1</sub>–HA<sub>1</sub> interface between influenza A and B virus HA prompted us to investigate the presence of internal cavities in these structures. Using the default outer probe radius of 10 Å in the 3V server (<http://3vee.molmovdb.org/>), we could not detect any internal cavity in influenza B virus HA. A small cavity of 485 Å<sup>3</sup> was located when we used a much smaller probe radius (5 Å) (Figure 6c and Table 2). This cavity is almost isolated from aqueous solution. Strikingly, by using the default value of 10 Å in all known

structures of influenza A virus HA proteins, we constantly found a large internal cavity that is beneath the HA<sub>1</sub> subunits, and just atop the C-terminus of the B-loop (Figure 6d and Table 2). These internal cavities are directly connected to the outside aqueous solution, indicating that protons could more easily diffuse into the interior of influenza A virus HA molecules than into influenza B virus HA.

The fusion peptide at the N-terminus of HA<sub>2</sub> in known structures of influenza B virus HA<sup>22,26,27</sup> is very different from that of influenza A virus HA. In influenza B virus HA, the fusion peptide points away from its own helix A and helix B to interact with those of a neighboring subunit via residues Phe-2 and Phe-3 (Figure 6e). The residues that surround the 3-fold axis of the molecule become Glu-113. The fusion peptide also adopts a lower position (toward the viral membrane) in the structure, thus losing most of the polar interactions with Asn-109 and Asp-112 (Figure 6g). In previous studies, it has been shown that compromised interactions between the fusion peptide and Asp-112 destabilized the protein, increased the fusion pH, and accelerated the kinetics of membrane fusion.<sup>13,14,19</sup> In sharp contrast, the fusion peptide of influenza A virus HA is located near the 3-fold symmetry axis of the molecule and forms a network of hydrophobic interactions at residues Leu-2 and Phe-3 (Figure 6f). In addition, the fusion peptide makes a total of six hydrogen bonds with Asp-112 and one hydrogen bond with Asp-109 (Figure 6h). Overall, the fusion peptide and its

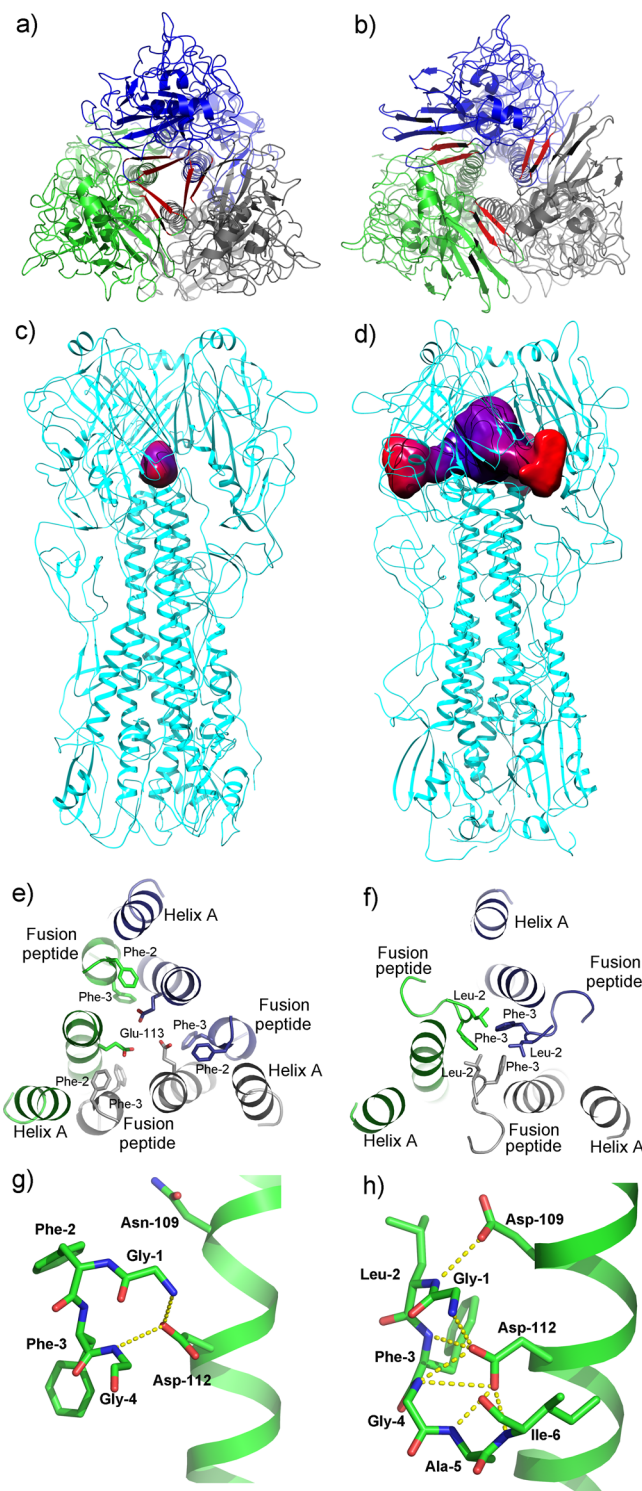


**Figure 6.** Comparison of prefusion structures of influenza A/H3N2 and B virus HA. Panels a, c, e, and g are for influenza B virus HA, while panels b, d, f, and h are for influenza A/H3N2 HA. (a and b) HA<sub>1</sub>–HA<sub>1</sub> interface. Each HA<sub>1</sub>–HA<sub>2</sub> subunit is separately colored. Two corresponding  $\beta$ -strands are colored red in both structures to highlight the different packing between them. (c and d) Internal cavity at the HA<sub>1</sub>–HA<sub>2</sub> interface. Different outer probe radius sizes were used, 5 Å for influenza B virus HA and 10 Å for influenza A/H3N2 HA. (e and f) Conformation of the fusion peptide. (g and h) Interactions between the fusion peptide and residues 109 and 112.

interacting residues are more exposed in influenza B virus HA than in influenza A virus HA.<sup>27</sup>

**Table 2. Comparison of Prefusion Structures of Influenza A and B Virus HA Proteins**

HA (PDB entry) <sup>a</sup>	orientation of the R domain relative to that of influenza B virus HA <sup>b</sup>		HA <sub>1</sub> –HA <sub>1</sub> interface area <sup>c</sup> (Å <sup>2</sup> )	cavity size <sup>d</sup> (Å <sup>3</sup> )	exposed surface area of the B-loop <sup>e</sup> (%)
	rotation (deg)	translation (Å)			
BHA (3BT6)	—	—	4052.7	485	22.4
<b>H1</b> (1RUZ)	58.5	0.3	2075.4	5082	40.8
<b>H2</b> (2WRC)	55.6	0.9	1723.5	8985	31.6
<i>H3</i> (3HMG)	33.2	3.4	2816.4	7299	36.2
<b>H5</b> (1JSM)	57.0	0.7	2610.6	5390	36.6
<i>H7</i> (1TI8)	27.8	3.8	2158.9	3477	34.9
<b>H9</b> (1JSD)	45.3	0.1	2753.7	3755	31.8
<b>H13</b> (4KPS)	48.9	0.9	2761.1	3654	30.3
<i>H14</i> (3EYJ)	34.4	3.0	2977.2	3978	36.4
<b>H17</b> (4I78)	42.7	−0.1	2971.2	7896	55.8

<sup>a</sup>Influenza A virus HA proteins are shown in bold for group 1 and italics for group 2. <sup>b</sup>The R domain (HA<sub>1</sub> residues 115–261) of different influenza A virus HAs was superposed with that of influenza B virus HA by the Dalilite server (<http://www.ebi.ac.uk/Tools/structure/dalilite/>). The HA<sub>2</sub> domains were aligned at HA<sub>2</sub> residues 37–55 and HA<sub>2</sub> residues 76–110. The orientation of the R domain was calculated by the Dyndomain server (<http://fizz.cmp.uea.ac.uk/dyndom/>). <sup>c</sup>The solvent accessible surface area (SASA) was analyzed by using InterProSurf server (<http://curie.utmb.edu/prosurf.html>). The HA<sub>1</sub>–HA<sub>1</sub> interface area was calculated by the formula SASA(three monomeric HA<sub>1</sub>) – SASA(trimeric HA<sub>1</sub>). <sup>d</sup>The cavity was found by the 3V server (<http://3vee.molmovdb.org/>). The default value for the outer probe radius (10 Å) was used for calculating the cavity size for influenza A virus HAs. For influenza B virus HA, the default value did not reveal any internal cavity. The reported internal cavity of 485 Å<sup>3</sup> was found using an outer probe radius of 5 Å. <sup>e</sup>The surface area was calculated using Areaimol in CCP4.

## DISCUSSION

Influenza A and B virus HA proteins belong to class I of the viral fusion proteins. Prior studies of the prefusion and postfusion structures of influenza A/H3N2 HA have revealed the extent of large-scale structural rearrangements that accompany the membrane fusion process. These include (a) the dissociation of HA<sub>1</sub>–HA<sub>1</sub> monomers, (b) the folding of region B from a loop conformation in the prefusion state to a helical conformation in the postfusion state, (c) the release of the fusion peptide from its burial site at the prefusion state to insert into the target membrane, and (d) the folding back of helix E to deliver the C-terminal transmembrane domain to the same end of the molecule as the fusion peptide.<sup>15,18</sup> Among these expected structural rearrangements, a recent study of an early fusion intermediate of influenza A/H2 HA suggested that steps a and b likely precede step c,<sup>38</sup> and a study of single influenza virions indicated that step c is a rate-limiting step in hemifusion with a decrease in pH.<sup>19</sup> However, we still lack an in-depth understanding of the molecular basis for these large-scale structural rearrangements.

With a low level of sequence identity with influenza A virus HA (at only ~20% for HA<sub>1</sub> and ~29% for HA<sub>2</sub> residues 31–181) and having diverged from each other some 2000 years ago,<sup>39</sup> influenza B virus HA can be regarded as a distant “cousin” to influenza A virus HA. A wealth of structures of influenza A virus HA subtypes H1–H3, H5, H7, H9, H13, H14, and H17<sup>17</sup> and influenza B virus HA<sup>22,26,27</sup> in the prefusion state and of influenza A/H3N2 HA in the postfusion state<sup>15,18</sup> exist. The newly determined structure of influenza B virus HA<sub>2</sub> in the postfusion state as reported here has filled an important structural gap in the field and allowed the identification of conserved features in the conformational changes of both influenza A and B virus HA. They appear to use similar pathways upon induction of acidic pH that serves to separate ionic residues strategically placed as clusters in prefusion structures.<sup>27,40</sup>

Despite the similar transition pathways shared between them, the detailed mechanisms used by influenza A and B virus HA proteins may differ. For instance, our structural analysis revealed that at the membrane distal end of the HA molecule, influenza A virus HA constantly has very loosely packed HA<sub>1</sub>–HA<sub>1</sub> interfaces compared to those of influenza B virus HA (Figure 6a,b and Table 2).<sup>27</sup> Probably related to this loose packing is the fact that influenza A virus HA proteins have large internal cavities at the HA<sub>1</sub>–HA<sub>2</sub> interface that is connected to the outside aqueous solution and contain B-loops that are more exposed than in influenza B virus HA (Figure 6c,d and Table 2). The transition from the prefusion state to the postfusion state of influenza HA can be described by the transition state theory, possibly via multiple intermediate states,<sup>38,41</sup> where the acidic pH serves to lower the transition state energy barrier(s).<sup>6</sup> This is presumably accomplished through protonation of ionizable residues strategically located at different locations throughout the protein to induce large-scale structural rearrangements.<sup>6,27,40</sup> Thus, some, if not all, of the structural features of influenza A virus HA mentioned above might lead to a higher sensitivity to pH changes or, in other words, decrease more substantially the transition state energy barrier(s) compared to that of influenza B virus HA. On the other hand, the less buried position of the fusion peptide in influenza B virus HA and its weakened interactions with Asp-112 and Asn-109 (Figure 6g,h), in conjunction with the higher helical propensity of the B-loop (Figure 1d), could result in lower transition state energy barriers, as shown by the structure of influenza A/H3N2 HA containing an Asp-112 → Gly mutation.<sup>42</sup> Recent studies clearly indicate a role of fusion pH in the pathogenicity and transmission of influenza virus.<sup>43–47</sup> On one hand, HA needs to have sufficient stability so that it is not activated prematurely, as evidenced by the contribution of stabilizing mutations in promoting airborne transmissibility of avian H5N1 virus.<sup>46,48</sup> On the other hand, highly pathogenic avian H5N1 virus tends to fuse at higher pH.<sup>44</sup> Therefore, systematically investigating the key chemical-structural elements that impact HA’s fusion pH and kinetics and their contributions to the pathogenicity and transmissibility of influenza virus is an urgent task. The new structure of influenza B virus HA<sub>2</sub> reported in this study and the common or unique structural features identified herein provide general guidance for such studies. Ultimately, studies along this line of research will provide a sound foundation for the development of next-generation antiviral fusion inhibitors.

## ASSOCIATED CONTENT

### Accession Codes

The coordinates and structure factors of the influenza B virus HA<sub>2</sub> structure reported in this study have been deposited as Protein Data Bank entry 4NKJ.

## AUTHOR INFORMATION

### Corresponding Author

\*E-mail: qinghuaw@bcm.edu. Phone: (713) 798-5289. Fax: (713) 796-9438.

### Funding

Q.W. acknowledges support from the National Institutes of Health (R01-AI067839), the Gillson-Longenbaugh Foundation, the Simmons Collaborative Research Fund Award from the Gulf Coast Consortium, and The Welch Foundation (Q-1826). Use of the Advanced Photon Source was supported by the U.S. Department of Energy, Basic Energy Sciences, Office of Science, under Contract DE-AC02-06CH11357. Use of BioCARS was also supported by the National Institute of General Medical Sciences of the National Institutes of Health via Grant R24GM111072.

### Notes

The authors declare no competing financial interest.

## REFERENCES

- (1) Sollner, T. H. (2004) Intracellular and viral membrane fusion: A uniting mechanism. *Curr. Opin. Cell Biol.* 16, 429–435.
- (2) Harrison, S. C. (2008) Viral membrane fusion. *Nat. Struct. Mol. Biol.* 15, 690–698.
- (3) Harrison, S. C. (2005) Mechanism of membrane fusion by viral envelope proteins. *Adv. Virus Res.* 64, 231–261.
- (4) White, J. M., Delos, S. E., Brecher, M., and Schornberg, K. (2008) Structures and mechanisms of viral membrane fusion proteins: Multiple variations on a common theme. *Crit. Rev. Biochem. Mol. Biol.* 43, 189–219.
- (5) Skehel, J. J., and Wiley, D. C. (1998) Coiled coils in both intracellular vesicle and viral membrane fusion. *Cell* 95, 871–874.
- (6) Skehel, J. J., and Wiley, D. C. (2000) Receptor binding and membrane fusion in virus entry: The influenza hemagglutinin. *Annu. Rev. Biochem.* 69, 531–569.
- (7) Wiley, D. C., and Skehel, J. J. (1987) The structure and function of the hemagglutinin membrane glycoprotein of influenza virus. *Annu. Rev. Biochem.* 56, 365–394.
- (8) Steinhauer, D. (2010) Influenza A virus haemagglutinin glycoproteins. In *Influenza: Molecular Virology* (Wang, Q., and Tao, Y. J., Eds.) pp 69–108, Caister Academic Press, Norfolk, U.K.
- (9) Klenk, H.-D., Rott, R., Orlich, M., and Blodorn, J. (1975) Activation of influenza A viruses by trypsin treatment. *Virology* 68, 426–439.
- (10) Lazarowitz, S. G., and Choppin, P. W. (1975) Enhancement of the infectivity of influenza A and B viruses by proteolytic cleavage of the hemagglutinin polypeptide. *Virology* 68, 440–454.
- (11) Lazarowitz, S. G., Compans, R. W., and Choppin, P. W. (1973) Proteolytic cleavage of the hemagglutinin polypeptide of influenza virus. Function of the uncleaved polypeptide HA. *Virology* 52, 199–212.
- (12) Webster, R. G., and Rott, R. (1987) Influenza virus A pathogenicity: The pivotal role of hemagglutinin. *Cell* 50, 665–666.
- (13) Daniels, P. S., Jeffries, S., Yates, P., Schild, G. C., Rogers, G. N., Paulson, J. C., Wharton, S. A., Douglas, A. R., Skehel, J. J., and Wiley, D. C. (1987) The receptor-binding and membrane-fusion properties of influenza virus variants selected using anti-haemagglutinin monoclonal antibodies. *EMBO J.* 6, 1459–1465.
- (14) Daniels, R. S., Downie, J. C., Hay, A. J., Knossow, M., Skehel, J. J., Wang, M. L., and Wiley, D. C. (1985) Fusion mutants of the influenza virus hemagglutinin glycoprotein. *Cell* 40, 431–439.

- (15) Bullough, P. A., Hughson, F. M., Skehel, J. J., and Wiley, D. C. (1994) Structure of influenza haemagglutinin at the pH of membrane fusion. *Nature* 371, 37–43.
- (16) Chen, J., Lee, K. H., Steinhauer, D. A., Stevens, D. J., Skehel, J. J., and Wiley, D. C. (1998) Structure of the hemagglutinin precursor cleavage site, a determinant of influenza pathogenicity and the origin of the labile conformation. *Cell* 95, 409–417.
- (17) Wilson, I. A., Skehel, J. J., and Wiley, D. C. (1981) Structure of the haemagglutinin membrane glycoprotein of influenza virus at 3 Å resolution. *Nature* 289, 366–373.
- (18) Chen, J., Skehel, J. J., and Wiley, D. C. (1999) N- and C-terminal residues combine in the fusion-pH influenza hemagglutinin HA<sub>2</sub> subunit to form an N cap that terminates the triple-stranded coiled coil. *Proc. Natl. Acad. Sci. U.S.A.* 96, 8967–8972.
- (19) Ivanovic, T., Choi, J. L., Whelan, S. P., van Oijen, A. M., and Harrison, S. C. (2013) Influenza-virus membrane fusion by cooperative fold-back of stochastically induced hemagglutinin intermediates. *Elife* 2, e00333.
- (20) Kilby, J. M., and Eron, J. J. (2003) Novel therapies based on mechanisms of HIV-1 cell entry. *N. Engl. J. Med.* 348, 2228–2238.
- (21) Rosenthal, P. B., Zhang, X., Formanowski, F., Fitz, W., Wong, C. H., Meier-Ewert, H., Skehel, J. J., and Wiley, D. C. (1998) Structure of the haemagglutinin-esterase-fusion glycoprotein of influenza C virus. *Nature* 396, 92–96.
- (22) Dreyfus, C., Laursen, N. S., Kwaks, T., Zuidgeest, D., Khayat, R., Ekiert, D. C., Lee, J. H., Metlagel, Z., Bujny, M. V., Jongeneelen, M., van der Vlugt, R., Lamrani, M., Korse, H. J., Geelen, E., Sahin, O., Sieuwerts, M., Brakenhoff, J. P., Vogels, R., Li, O. T., Poon, L. L., Peiris, M., Koudstaal, W., Ward, A. B., Wilson, I. A., Goudsmit, J., and Friesen, R. H. (2012) Highly conserved protective epitopes on influenza B viruses. *Science* 337, 1343–1348.
- (23) Ekiert, D. C., Bhabha, G., Elsliger, M. A., Friesen, R. H., Jongeneelen, M., Throsby, M., Goudsmit, J., and Wilson, I. A. (2009) Antibody recognition of a highly conserved influenza virus epitope. *Science* 324, 246–251.
- (24) Ekiert, D. C., Friesen, R. H., Bhabha, G., Kwaks, T., Jongeneelen, M., Yu, W., Ophorst, C., Cox, F., Korse, H. J., Brandenburg, B., Vogels, R., Brakenhoff, J. P., Kompiere, R., Koldijk, M. H., Cornelissen, L. A., Poon, L. L., Peiris, M., Koudstaal, W., Wilson, I. A., and Goudsmit, J. (2011) A highly conserved neutralizing epitope on group 2 influenza A viruses. *Science* 333, 843–850.
- (25) Wang, Q., Tian, X., Chen, X., and Ma, J. (2007) Structural basis for receptor specificity of influenza B virus hemagglutinin. *Proc. Natl. Acad. Sci. U.S.A.* 104, 16874–16879.
- (26) Ni, F., Kondashkina, E., and Wang, Q. (2013) Structural basis for the divergent evolution of influenza B virus hemagglutinin. *Virology* 446, 112–122.
- (27) Wang, Q., Cheng, F., Lu, M., Tian, X., and Ma, J. (2008) Crystal Structure of Unliganded Influenza B Virus Hemagglutinin. *J. Virol.* 82, 3011–3020.
- (28) Powell, H. R. (1999) The Rossmann Fourier autoindexing algorithm in MOSFLM. *Acta Crystallogr. D55*, 1690–1695.
- (29) Leslie, A. G. (2006) The integration of macromolecular diffraction data. *Acta Crystallogr. D62*, 48–57.
- (30) Collaborative Computational Project, Number 4 (1994) The CCP4 suite: Programs for protein crystallography. *Acta Crystallogr. D50*, 760–763.
- (31) Adams, P. D., Afonine, P. V., Bunkoczi, G., Chen, V. B., Davis, I. W., Echols, N., Headd, J. J., Hung, L. W., Kapral, G. J., Gross-Kunstleve, R. W., McCoy, A. J., Moriarty, N. W., Oeffner, R., Read, R. J., Richardson, D. C., Richardson, J. S., Terwilliger, T. C., and Zwart, P. H. (2010) PHENIX: A comprehensive Python-based system for macromolecular structure solution. *Acta Crystallogr. D66*, 213–221.
- (32) Emsley, P., and Cowtan, K. (2004) Coot: Model-building tools for molecular graphics. *Acta Crystallogr. D60*, 2126–2132.
- (33) Murshudov, G. N., Vagin, A. A., and Dodson, E. J. (1997) Refinement of macromolecular structures by the maximum-likelihood method. *Acta Crystallogr. D53*, 240–255.
- (34) Harrison, J. S., Koellhoffer, J. F., Chandran, K., and Lai, J. R. (2012) Marburg virus glycoprotein GP2: pH-dependent stability of the ectodomain α-helical bundle. *Biochemistry* 51, 2515–2525.
- (35) Koellhoffer, J. F., Malashkevich, V. N., Harrison, J. S., Toro, R., Bhosle, R. C., Chandran, K., Almo, S. C., and Lai, J. R. (2012) Crystal structure of the Marburg virus GP2 core domain in its postfusion conformation. *Biochemistry* 51, 7665–7675.
- (36) Weis, W. I., Brunger, A. T., Skehel, J. J., and Wiley, D. C. (1990) Refinement of the influenza virus hemagglutinin by simulated annealing. *J. Mol. Biol.* 212, 737–761.
- (37) Cohen, F. S., and Melikyan, G. B. (2004) The energetics of membrane fusion from binding, through hemifusion, pore formation, and pore enlargement. *J. Membr. Biol.* 199, 1–14.
- (38) Xu, R., and Wilson, I. A. (2011) Structural characterization of an early fusion intermediate of influenza virus hemagglutinin. *J. Virol.* 85, 5172–5182.
- (39) Suzuki, Y., and Nei, M. (2002) Origin and evolution of influenza virus hemagglutinin genes. *Mol. Biol. Evol.* 19, 501–509.
- (40) Wang, Q. (2010) Influenza Type B Virus Haemagglutinin: Antigenicity, Receptor Binding and Membrane Fusion. In *Influenza: Molecular Virology* (Wang, Q., and Tao, Y. J., Eds.) pp 29–52, Caister Academic Press, Norfolk, U.K.
- (41) Jasanoff, A. (1998) Structure and interactions of the invariant chain, pp 168, Harvard University, Cambridge, MA.
- (42) Weis, W. I., Cusack, S. C., Brown, J. H., Daniels, R. S., Skehel, J. J., and Wiley, D. C. (1990) The structure of a membrane fusion mutant of the influenza virus haemagglutinin. *EMBO J.* 9, 17–24.
- (43) Galloway, S. E., Reed, M. L., Russell, C. J., and Steinhauer, D. A. (2013) Influenza HA subtypes demonstrate divergent phenotypes for cleavage activation and pH of fusion: Implications for host range and adaptation. *PLoS Pathog.* 9, e1003151.
- (44) DuBois, R. M., Zaraket, H., Reddivari, M., Heath, R. J., White, S. W., and Russell, C. J. (2011) Acid stability of the hemagglutinin protein regulates HSN1 influenza virus pathogenicity. *PLoS Pathog.* 7, e1002398.
- (45) Reed, M. L., Bridges, O. A., Seiler, P., Kim, J. K., Yen, H. L., Salomon, R., Govorkova, E. A., Webster, R. G., and Russell, C. J. (2010) The pH of activation of the hemagglutinin protein regulates HSN1 influenza virus pathogenicity and transmissibility in ducks. *J. Virol.* 84, 1527–1535.
- (46) Herfst, S., Schrauwen, E. J., Linster, M., Chutinimitkul, S., de Wit, E., Munster, V. J., Sorrell, E. M., Bestebroer, T. M., Burke, D. F., Smith, D. J., Rimmelzwaan, G. F., Osterhaus, A. D., and Fouchier, R. A. (2012) Airborne transmission of influenza A/HSN1 virus between ferrets. *Science* 336, 1534–1541.
- (47) Imai, M., Watanabe, T., Hatta, M., Das, S. C., Ozawa, M., Shinya, K., Zhong, G., Hanson, A., Katsura, H., Watanabe, S., Li, C., Kawakami, E., Yamada, S., Kiso, M., Suzuki, Y., Maher, E. A., Neumann, G., and Kawaoka, Y. (2012) Experimental adaptation of an influenza H5 HA confers respiratory droplet transmission to a reassortant H5 HA/H1N1 virus in ferrets. *Nature* 486, 420–428.
- (48) Yamada, S., Suzuki, Y., Suzuki, T., Le, M. Q., Nidom, C. A., Sakai-Tagawa, Y., Muramoto, Y., Ito, M., Kiso, M., Horimoto, T., Shinya, K., Sawada, T., Usui, T., Murata, T., Lin, Y., Hay, A., Haire, L. F., Stevens, D. J., Russell, R. J., Gamblin, S. J., Skehel, J. J., and Kawaoka, Y. (2006) Haemagglutinin mutations responsible for the binding of HSN1 influenza A viruses to human-type receptors. *Nature* 444, 378–382.